Controlling anisotropic properties by manipulating the orientation of chiral small molecules

Jessica Wade[1,2*], Francesco Salerno[2,3†], Rachel C. Kilbride[4†], Dong Kuk Kim[1,2], Julia A. Schmidt[3], Joel A. Smith[5], Luc M. LeBlanc[6], Emma Wolpert[2,3], Adebayo A. Adeleke[6], Erin R. Johnson[6], Jenny Nelson[2,7], Tadashi Mori[8], Kim Jelfs[2,3], Sandrine Heutz[1,2] and Matthew J. Fuchter[2,3*]

[1] Department of Materials and London Centre of Nanotechnology, Imperial College London, Exhibition Road, London SW7 2AZ, United Kingdom

[2] Centre for Processable Electronics, Imperial College London, Exhibition Road, London SW7 2AZ, United Kingdom

[3] Department of Chemistry and Molecular Sciences Research Hub, Imperial College London, White City Campus, 82 Wood Lane, London W12 0BZ, United Kingdom

[4] Department of Physics and Astronomy, The University of Sheffield, Hicks Building, Hounsfield Road, Sheffield, S3 7RH, United Kingdom

[5] Department of Physics, Clarendon Laboratory, University of Oxford, Oxford, OX1 3PU, United Kingdom

[6] Department of Chemistry, Dalhousie University, 6274 Coburg Road, Halifax, Nova Scotia, Canada B3H 4R2

[7] Department of Physics, Imperial College London, Exhibition Road, London SW7 2AZ, United Kingdom

[8] Department of Applied Chemistry, Graduate School of Engineering, Osaka University 2-1 Yamada-oka, Suita, Osaka 565-871, Japan

E-mail: jessica.wade@imperial.ac.uk; m.fuchter@imperial.ac.uk

[†] These authors contributed equally to this work.

# Contents

Supplementary Notes. CN6H synthesis

Reagents and solvents were purchased from commercial sources (Fluorochem, Sigma-Aldrich, and TCI) and used without further purification. Reactions were monitored by thin layer chromatography (Merck silica gel 0.25 mm) with visualization under UV irradiation at 254 nm and 365 nm. Flash chromatography was performed using silica gel (Fluorochem, 60 Å, 230-400 mesh). Flow photochemical reactions were performed with an R-series Vapourtec UV-150 flow microreactor equipped with a 365 nm high power LED lamp. The flow system was part of and used with permission of the ROAR (Centre for Rapid Online Analysis of Reactions) at Imperial College London. The synthesis of the 2,2'-dicyano[6]helicene was performed in two steps:
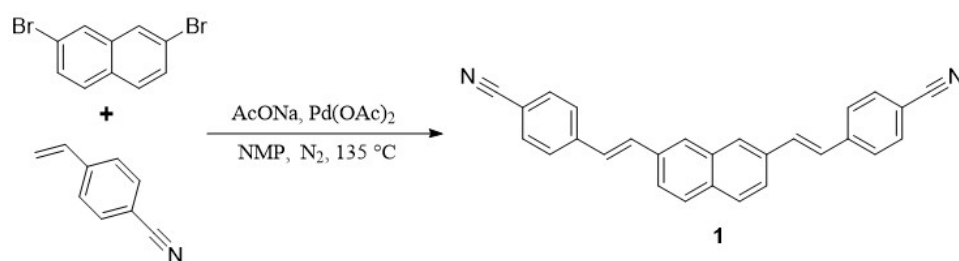
2-7-Bis(4-cyanostyryl)naphthalene (1)[1]

2,7-Dibromonaphthalene (2.55 g, 8.92 mmol, 1 equiv.), dry sodium acetate (1.61 g, 19.62 mmol, 2.2 equiv.) and 4-cyanostyrene (3.00 g, 23.19 mmol, 2.6 equiv.) were added under nitrogen in a 250 mL flask with 20 mL of dry N-methyl-2-pyrrolidone (NMP). The mixture was deaerated by sparging with N_2 for 1 hour and then heated to 120 °C. In a separate flask, a 10 mL NMP solution of palladium acetate (8 mg) was prepared under nitrogen. After deaerating this solution for 20 min, 2.5 mL (0.001 equiv, 0.1% mol) were transferred to the reaction flask. The temperature was then increased to 135 °C. After 72 hours, the flask was then cooled down to RT and an excess of water was added. The solution was filtered through a Buchner filter and the yellow powder collected and washed with DCM and the solid recrystallized from a mixture DCM/acetone/MeOH ca 2/1/1 to obtain **1**. The remaining solution was concentrated to dryness and the crude further purified by column chromatography on silica gel with gradient solvent system CH_2Cl_2/pentane 6/4 to CH_2Cl_2. Rf = 0.6 (CH_2Cl_2). Total yield 65% (*E/E* isomer). ^{1}H-NMR (400 MHz, CDCl3) δ ppm: 7.90 (s, 2H), 7.87 (d, J = 8.4 Hz; 2H), 7.77 (d, J = 8.4 Hz; 2H), 7.68 (m, 8H), 7.41 (d, J = 8.4 Hz; 2H), 7.26 (d, J = 8.4 Hz; 2H). ^{13}C-NMR (400 MHz, CDCl3) δ ppm: 110.8, 118.9, 123.6, 124.0, 127.0, 127.4, 127.7, 128.4, 132.2,

132.6, 133.4, 134.6, 133.8, 141.7. CI-HRMS m/z theoretical mass for $C_{28}H_{19}N_2^+$: 383.1543, found: 383.1540.

1 → UV-A, toluene / I_2, O_2, → **CN6H**
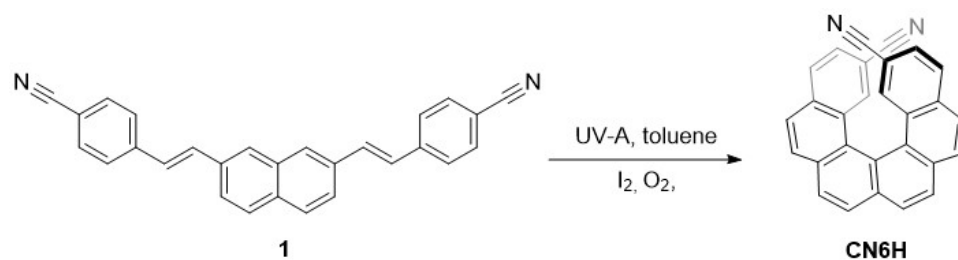
(±)-2,2'-dicyano[6]helicene (CN6H)[1]

Precursor **1** (530 mg, 1.39 mmol, 1 equiv.) and I_2 (52 mg, 0.21 mmol, 0.15 equiv.) were dissolved in 2.2 L of toluene. The solution was stirred for 1 hour to allow the substrate to dissolve [note, it never dissolved completely and was used as a fine suspension]. The solution was pumped by a peristaltic pump at 2 mL/min through the flow reactor. Exposure time to UV light (365 nm) was 5 minutes, temperature 60 °C. After *ca* 8 h, the total collected solution collected was evaporated and the solid triturated with AcOEt overnight to afford 215 mg of pure racemic product **CN6H** (41 % yield).

Chiral resolution was performed by the company Reach Separations using a column Lux iA3 21.2 x 250mm, 5 μm. Temperature 40 °C, flow rate of 50 mL/min, isocratic conditions MeOH/scCO$_2$ 35/65. 500 μL of the compound dissolved in Toluene/DCM 2/1 at a 3.5 mg/mL concentration was injected and the products detected at 275 nm. 617 mg of racemic CN6H were injected in total to obtain 113 mg of enantiomer 1 (*P*), 171 mg of enantiomer 2 (*M*), both with *ee* > 99%, and a third scalemic fraction (241 mg). The overall yield was lower than expected due to the low solubility of the molecule.

Supplementary Figure 1. CN6H single crystal structure
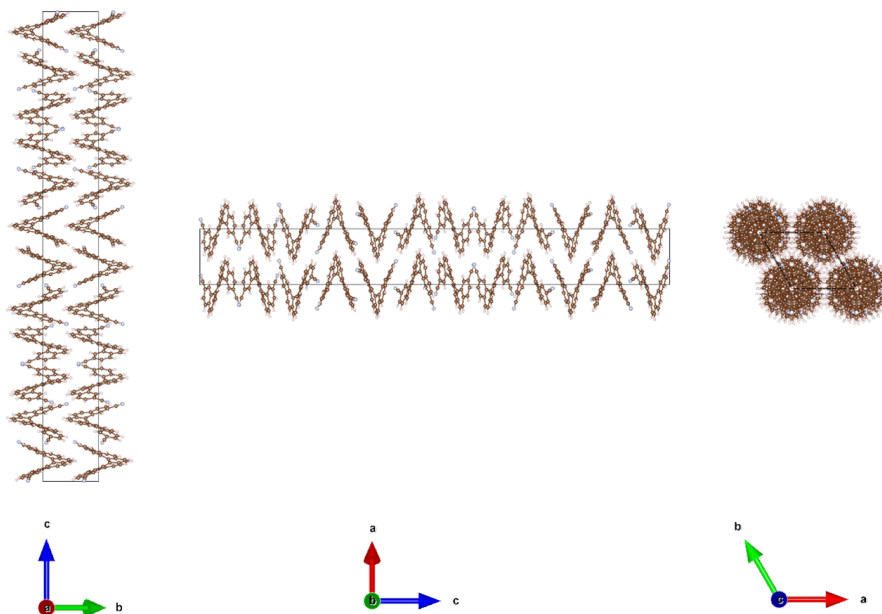
The bis-2,2'-cyano[6]helicene (**CN6H**) crystallises as a conglomerate in UJOCOL characterised by helicene molecules arranged into enantiopure supramolecular columns. The unit cell is highly anisotropic and the crystal is hexagonal uniaxial.
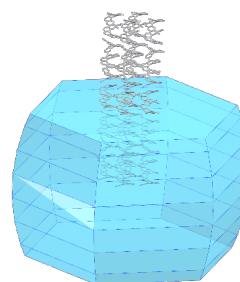
Space Group: P6$_1$22 (178)

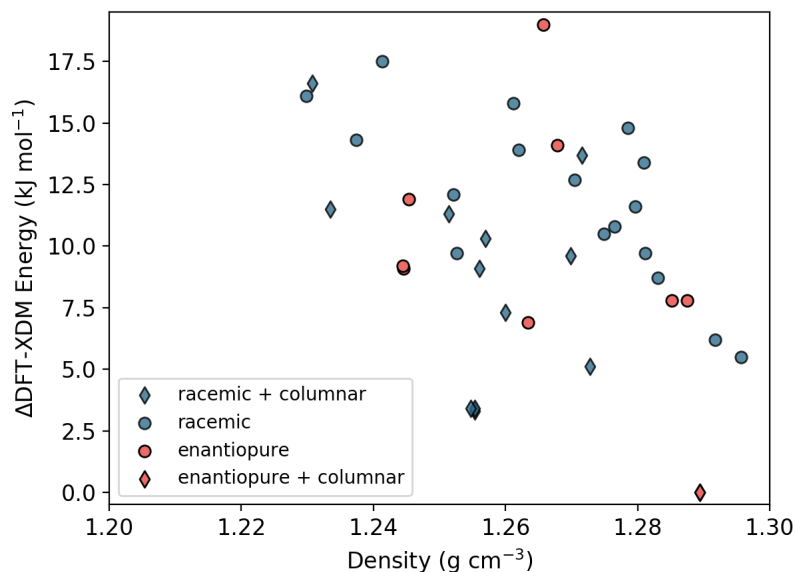$$a = 9.73600 \text{ Å} \quad \alpha = 90.0000°$$

$$b = 9.73600 \text{ Å} \quad \beta = 90.0000°$$

$$c = 70.73100 \text{ Å} \quad \gamma = 120.0000°$$

$$V = 5806.3282 \text{ Å}^3$$

Hexagonal:

$$a = b \neq c$$

$\alpha = \beta = 90° (\gamma = 120°)$

Supplementary Discussion 1. Crystal structure prediction

Crystal-energy landscape of the lowest-lying polymorphs obtained from the CN6H CSP search and relaxed at DFT-XDM level of theory. Racemic polymorphs are shown in blue whilst enantiopure polymorphs are shown in red. If the polymorph contains columnar packing, a diamond shape is used. If it does not, a circular shape is used. The experimentally observed polymorph is the only low-lying polymorph showing homochiral columnar packing (red diamonds).
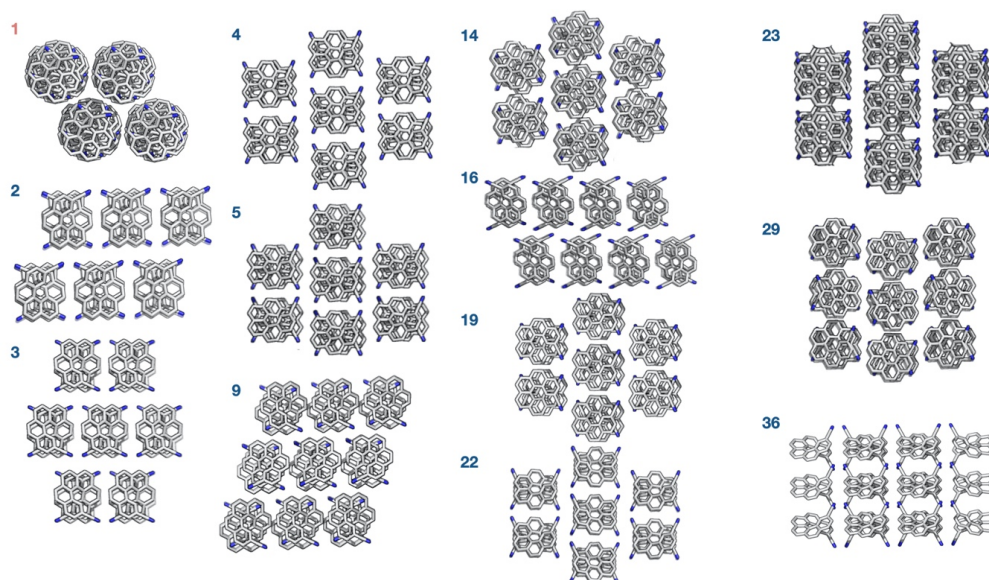
An illustration of the polymorphs showing columnar packing. The polymorphs are numbered by their relative position in the crystal-energy landscape starting from the global minimum structure (structure 1). The $P6_122$ polymorph is the only polymorph with homochiral columnar packing (structure 1, red). All remaining polymorphs with columnar packing are heterochiral

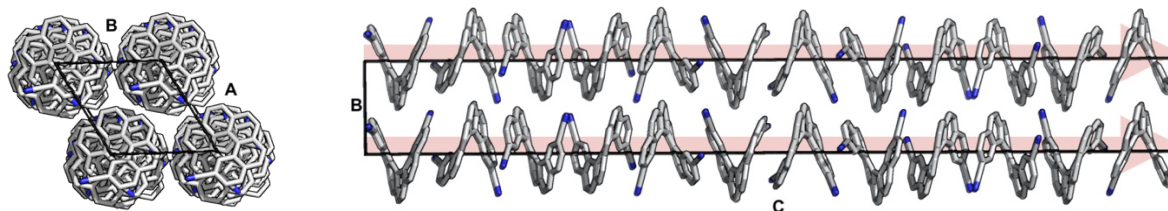(blue). Carbon atoms are coloured in grey, nitrogen atoms in blue and hydrogens are omitted for clarity.
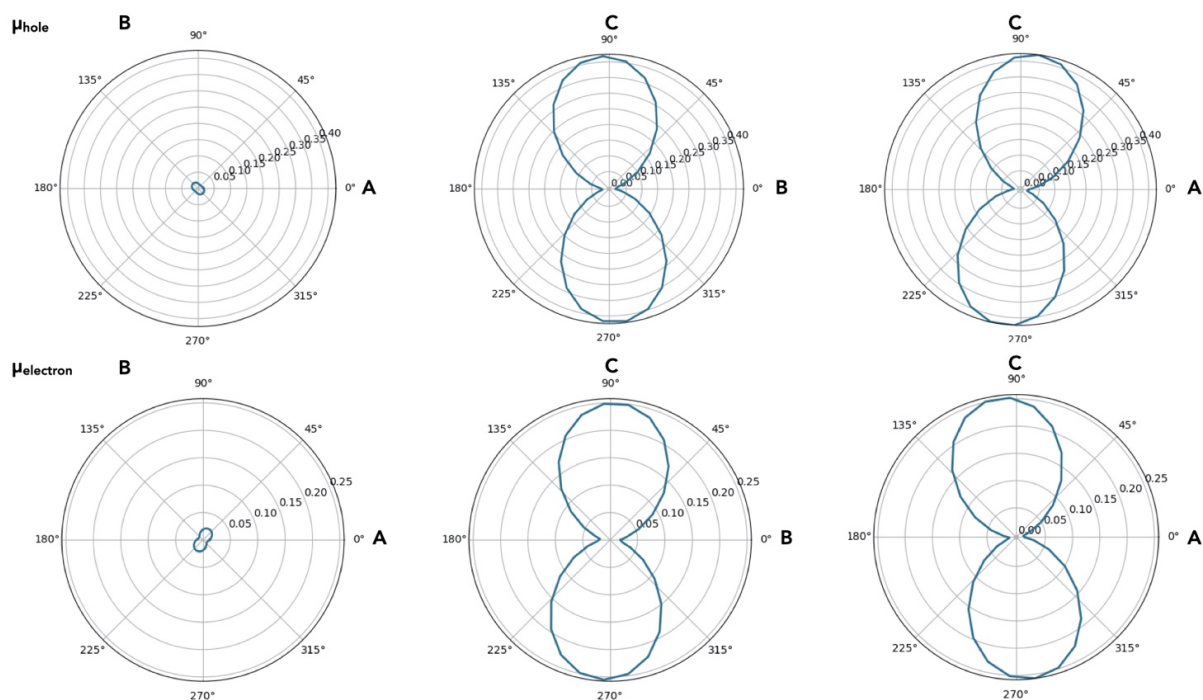
Angular-dependent charge-mobility plots of the CN6H of structure 1 (CSD reference code: UJOCOL, P6$_1$22 symmetry) hole and electron mobilities in cm^2 V^{-1} s^{-1}.

Structure 1 (CSD reference code: UJOCOL, P6122 symmetry) along the ab- (left) and bc-plane (right). There is little/no charge transport along the ab-plane, but significant charge transport along the homochiral column in the bc- and ac-planes.

Supplementary Figure 2. Powder XRD Simulation
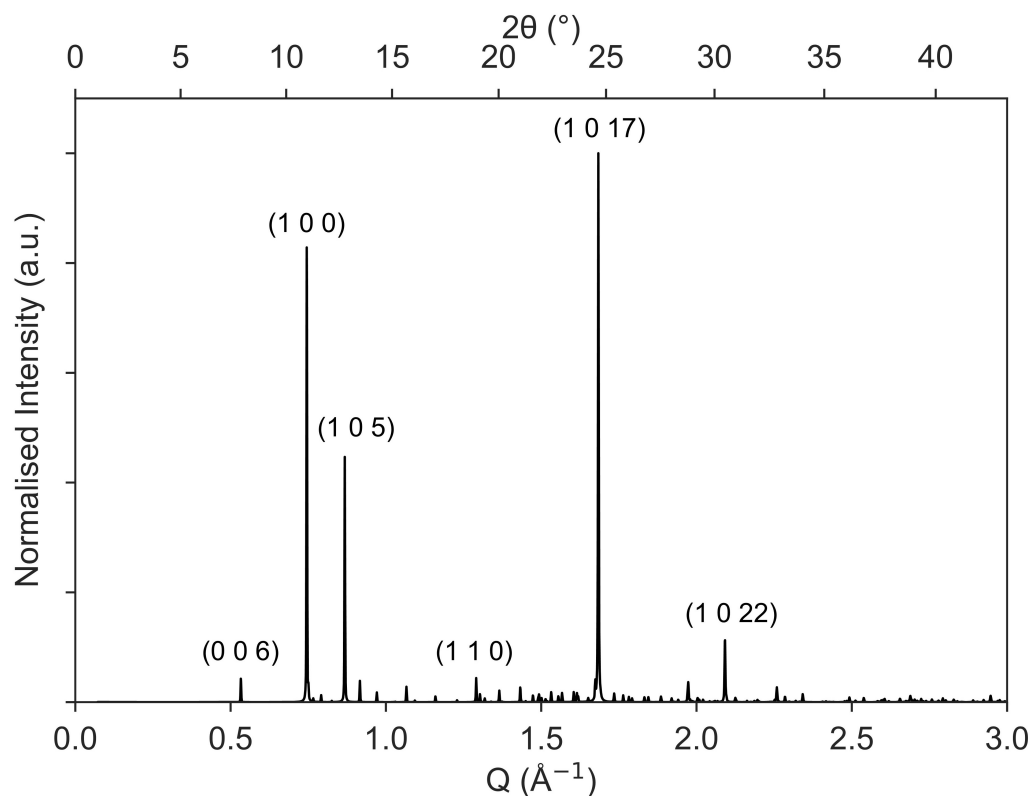
Powder XRD data of CN6H single crystal structure simulated using a previously reported crystallographic information file (CIF)[2]. Intensities are normalised to maximum intensity and the miller indices (hkl) of the highest intensity reflections are labelled. 2θ values are converted to Q using $Q = \frac{4\pi sin\theta}{\lambda}$ where λ = 1.5406 Å.

Supplementary Table 1. Reflections from simulated powder XRD patterns.

h	k	l	d (Å)	2θ (°)	Q (Å⁻¹)	Normalised Intensity	Multiplicity
1	0	17	3.73	23.83	1.68	100.00	12
1	0	0	8.43	10.48	0.75	67.63	6
1	0	5	7.24	12.21	0.87	36.29	12
1	0	22	3.00	29.72	2.09	13.09	12
1	1	0	4.87	18.21	1.29	3.96	6
0	0	6	11.79	7.49	0.53	3.30	2
1	0	6	6.86	12.90	0.92	3.20	12
1	0	24	2.78	32.15	2.26	3.17	12
1	1	12	3.75	23.69	1.67	3.13	12
1	0	34	2.02	44.84	3.11	2.84	12
1	1	7	4.39	20.23	1.43	2.52	12
0	0	12	5.89	15.02	1.07	2.41	2
1	1	5	4.60	19.27	1.36	1.98	12
1	0	16	3.92	22.69	1.60	1.80	12
2	0	4	4.10	21.65	1.53	1.78	12
1	1	22	2.68	33.37	2.34	1.74	12
2	1	1	3.18	28.00	1.97	1.69	12
1	2	1	3.18	28.00	1.97	1.69	12
2	1	0	3.19	27.98	1.97	1.68	12

Table of the highest intensity reflections from the simulated powder XRD pattern shown above.

Supplementary Discussion 2. *Lattice Plane Guide*: Face-On
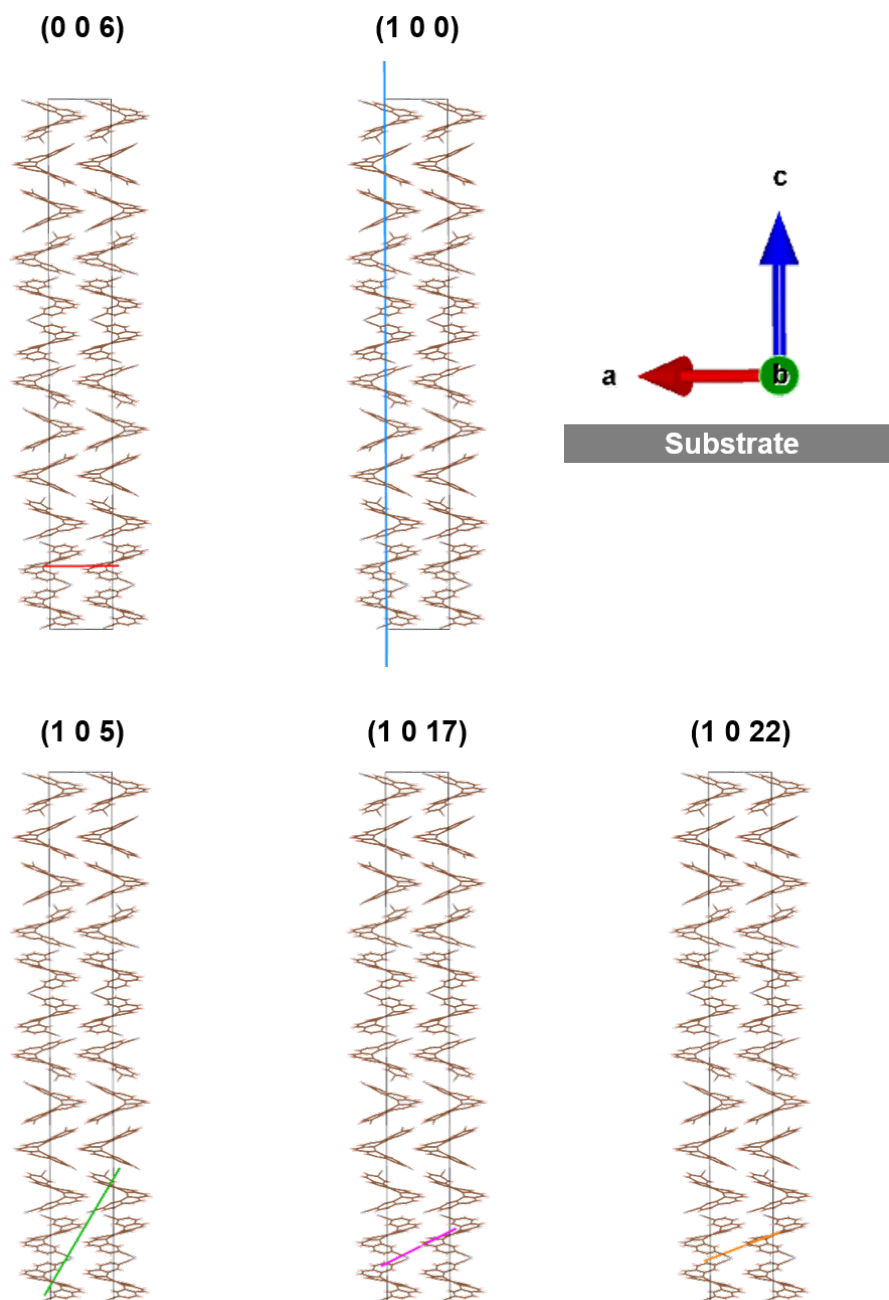
An illustration of the alignment of the (0 0 6), (1 0 0), (1 0 5), (1 0 17) and (1 0 22) lattice planes for face-on oriented **CN6H**. Out-of-plane diffraction is expected for the (0 0 6), (1 0 17) and (1 0 22) planes as they are aligned parallel to the substrate and so are expected to be observed in XRD operated in the Q-2Q mode. The (1 0 0) plane is aligned perpendicular to the substrate, diffracting in the in-plane direction so is not expected to be observed in this diffraction mode. The (1 0 5) plane is not aligned parallel or perpendicular to the substrate so is not expected to be observed in XRD for either face-on or edge-on orientation.

Lattice Plane Guide: Edge-On

(0 0 6)

(1 0 0)

(1 0 5)
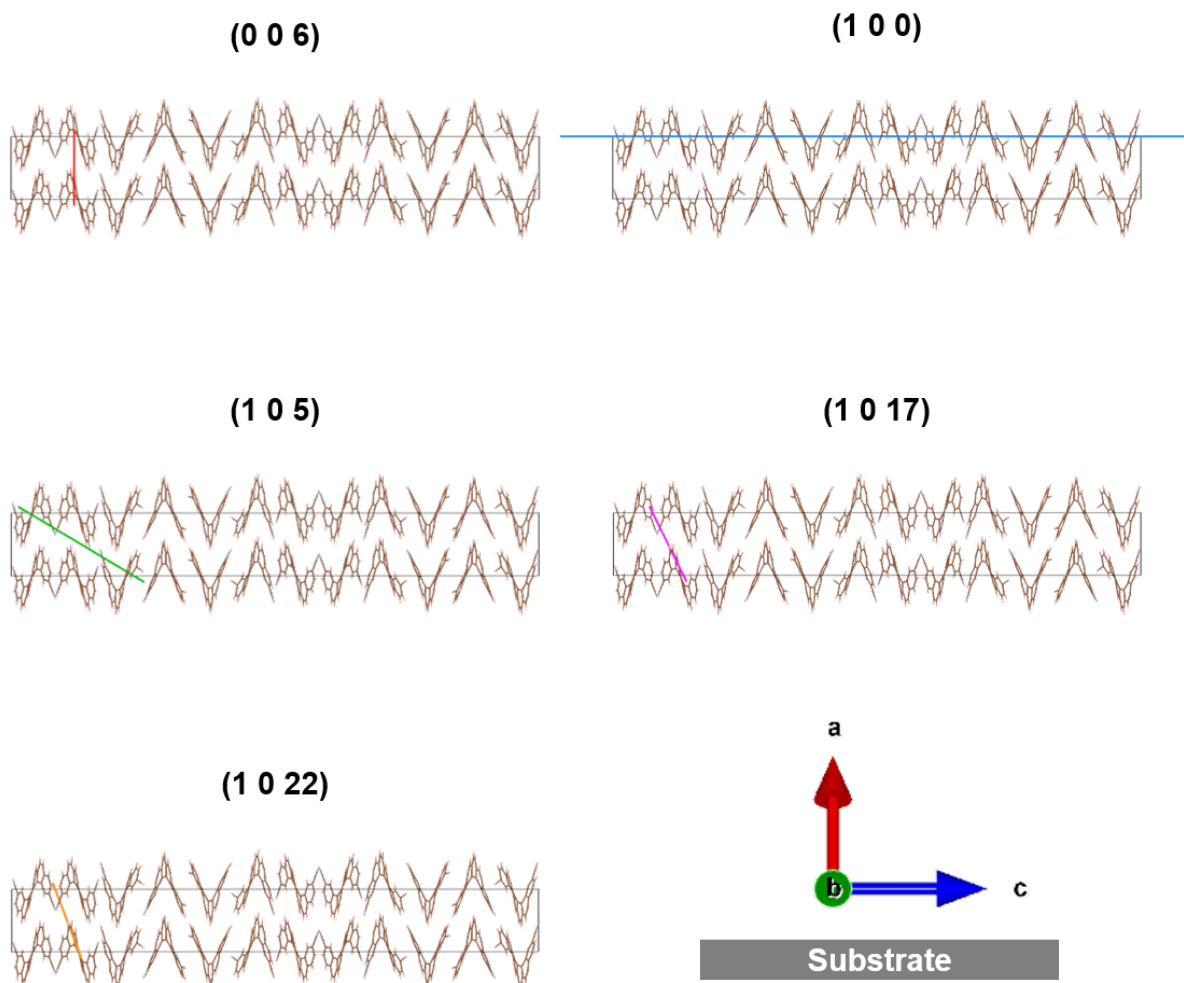
(1 0 17)

(1 0 22)

An illustration of the alignment of the (0 0 6), (1 0 0), (1 0 5), (1 0 17) and (1 0 22) lattice planes for edge-on oriented **CN6H**. Out-of-plane diffraction is expected for the (1 0 0) plane as it is aligned parallel to the substrate and so is expected to be observed in Q – 2Q XRD. The (0 0 6), (1 0 17) and (1 0 22) planes are aligned perpendicular or almost perpendicular to the substrate, diffracting in the in-plane direction so are not expected to be observed in XRD. The (1 0 5) plane is not aligned parallel or perpendicular to the substrate so is not expected to be observed in XRD for either face-on or edge-on orientation.

# Supplementary Table 2. 2D GIWAXS Simulation Parameters

Sample	Reciprocal axis oriented along Qz	χ angles to probe (°)	Width of out-of-plane distribution $W_\perp$ (°)	Line shape of out-of-plane distribution $\mu_\perp$
CN6H [*M*] on bare silicon	1 0 17	-90:1:90	360	0.9
CN6H [*P*] on bare silicon	0 0 1 (0 0 6)	-90:1:90	360	0.9
CN6H [*M*] on PTCDA	0 0 1 (0 0 6)	-60:1:60	120	0.5
CN6H [*M*] on CuI	1 0 0	-35:0.5:35	15	0.4

SimDiffraction parameters used to simulate 2D GIWAXS scattering patterns with a Pseudo-Voigt (PSV) model. Here the reciprocal axis along Q_z describes the primary orientation, χ angles are the range of probed crystallite tilts away from this orientation, $W_\perp$ describes the width of the PSV distribution and $\mu_\perp$ is the proportion of Gaussian or Lorentzian contribution to the PSV model ($\mu_\perp=0$ is Gaussian and $\mu_\perp=1$ is Lorentzian). For each simulation, a number of corrections were applied; specular Lorentz correction, isotropic polarisation correction, Yoneda correction and structure factor correction determined from relative atomic positions. The following *SimDiffraction* parameters were kept constant for each simulation: the instrumental peak width (0.03Å^{-1}), peak shape (0.2), in-plane correlation length (100Å) and layers (d = 40Å, n=8). See the *SimDiffraction* software manual for further details.[3]

Supplementary Figure 3. GIWAXS of Bare Substrates
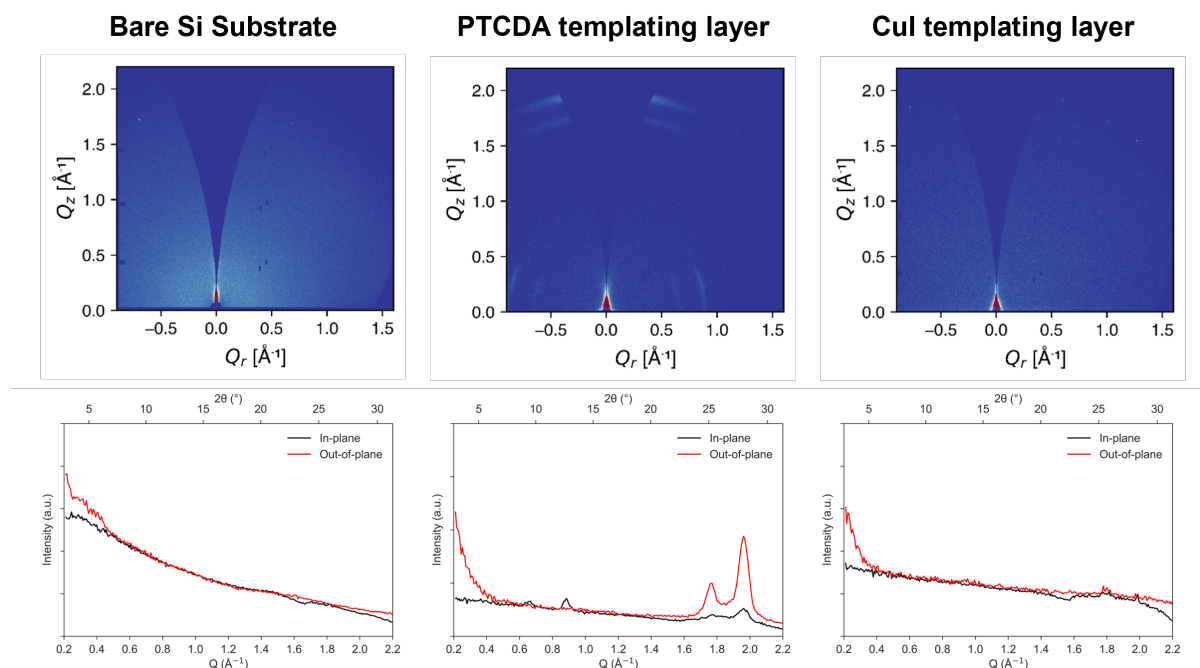
2D GIWAXS patterns of the bare substrates and corresponding 1D Q-dependent profiles integrated in the range 0.2 Å⁻¹ ≤ Q ≤ 2.2 Å⁻¹ through various χ angles; out-of-plane (in the Qz direction, χ= 0°±20°) and in-plane (which includes all other angles 20° ≤ χ ≤ 90°).

Silicon and CuI-templated silicon display no prominent scattering features in the observable Q-range. It should be noted that scattering of the (1 1 -1) and (2 0 0) CuI lattice planes falls outside the observable in-plane Q range in this work (0.2 $Å^{-1}$< Q < 2.2$Å^{-1}$). For PTCDA, previous studies have reported the existence of two crystalline polymorphs which form herringbone-like structures.[4] The PTCDA films used in this work displays an *α*-crystalline structure in the monoclinic *P*2$_1$/*c* space group. The PTCDA molecules adopt a flat-lying orientation with the conjugated backbones aligned parallel to the substrate separated by an intermolecular spacing of d = 3.22Å (out-of-plane peak at Q = 1.95Å⁻¹) in agreement with previous results.[5]

Supplementary Discussion 3. 2D GIWAXS Peak Indexing

An unoriented film will exhibit little dependence on the azimuthal angle χ away from the normal, out-of-plane direction (appearing as completely isotropic scattering rings in the 2D pattern). In the figure we show 2D data remapped as a function of χ for t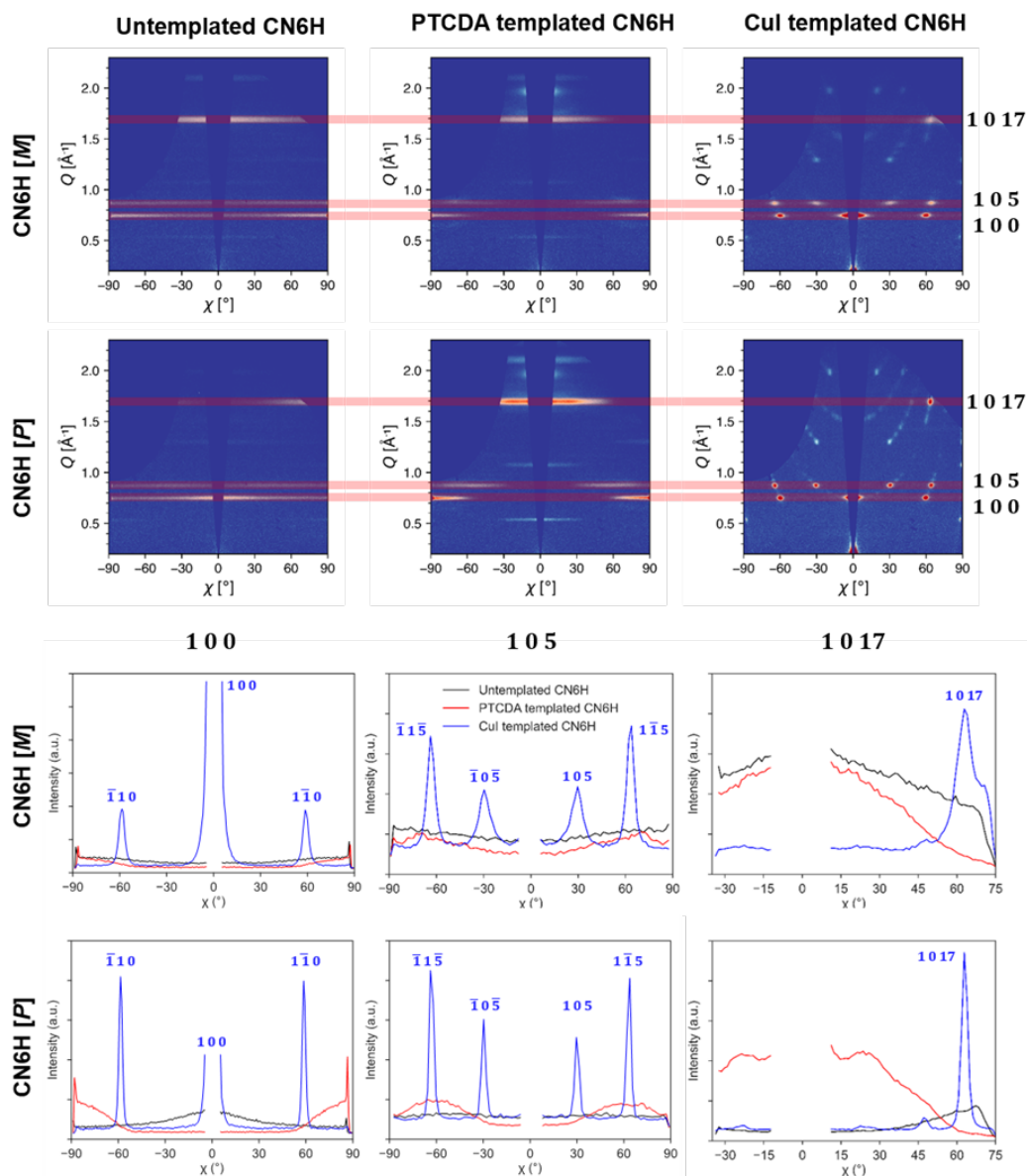emplated and untemplated **CN6H** with 1D χ-dependent intensity profiles. χ is defined as the angle normal to the beam incidence at the detector (χ = 0° is the out-of-plane direction and χ = ± 90° is the in-plane direction). These profiles are the integrated scattering intensity over Q
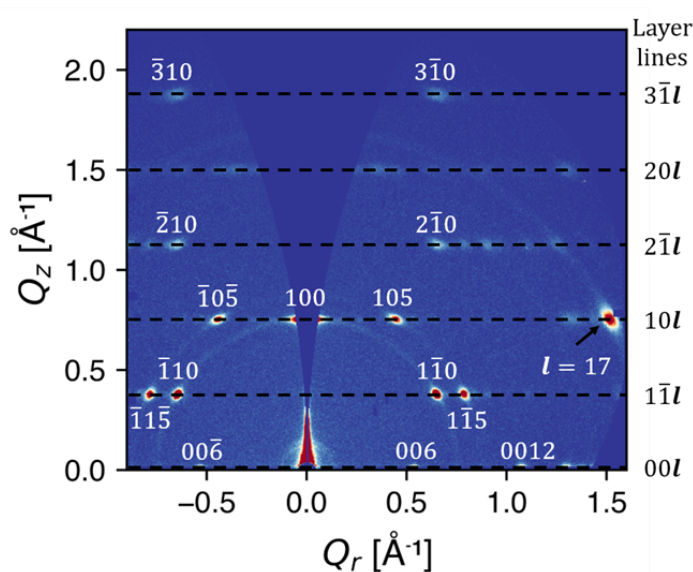
*2D peak indexing of CuI-templated **CN6H** [P] with miller indices and fibre diffraction layer lines labelled. Indexing was assisted using the GIXSGUI Matlab toolbox[14].*

ranges corresponding to the (1 0 0), (1 0 5) and (1 0 17) lattice planes. For untemplated **CN6H**, although the reflections appear as weak intensity rings, there is some angular dependence. In agreement with the 2D simulations described above, there is a very broad distribution of (1 0 17) in the out-of-plane direction, which suggests multiple weakly-ordered crystallite orientations. For PTCDA-templated **CN6H**, a peak can be seen at χ ~ ±90° in the χ-dependent azimuthally integrated profile of the (1 0 0) plane and a peak at χ ~ 25° in the (1 0 17) profile. This confirms the dominant face-on orientation, however the broad distribution in the azimuthal profiles indicates that there are also several other orientations present. The highly ordered orientation of CuI-templated **CN6H** is demonstrated by the appearance of sharp peaks in the χ-dependent intensity profiles. In the (1 0 0) profile, peaks are observed in the out-of-plane direction (χ = 0°) and at χ ~ ±60°. This is expected for a uniaxial, edge-on orientation of **CN6H** supramolecular and is understood by considering symmetry equivalent planes for the 1 0 0 reflection which has a multiplicity of 6 in the hexagonal system. With only weak scattering away from the primary orientations, the CuI-templated films are both close to uniaxially, edge-on oriented.

Supplementary Figure 4. Azimuthal 2D Reshaped Images and χ-dependent integrations

*2D azimuthal reshaped GIWAXS patterns of untemplated and templated **CN6H** [M] and **CN6H** [P]. Below are azimuthally integrated χ-dependent 1D profiles performed across the full χ range in the red shaded regions at Q-ranges of 0.65 Å⁻¹ ≤ Q ≤ 0.8 Å⁻¹, 0.8 Å⁻¹ ≤ Q ≤ 0.9 Å⁻¹ and 1.64 Å⁻¹ ≤ Q ≤ 1.74 Å⁻¹ to probe the orientation of the (1 0 0), (1 0 5) and (1 0 17) lattice planes respectively. Additional peaks in the 1 0 0 profile for CuI-templated **CN6H** correspond to reflections from symmetry equivalent planes (1 0 0), (0 1 0), (-1 0 0), (0 -1 0), (1 -1 0) and (-1 1 0) which are separated by a reciprocal angle γ*=60° (i.e. separated by χ = 60° on the detector). Similarly in the 1 0 5 profile, additional peaks are observed for the symmetry equivalent planes which includes the (1 -1 5) plane (indexed above).*

Supplementary Discussion 4. Simulations of molecule – surface interactions

The CuI surface model was constructed starting from the experimental crystal structure (COD ID: 1011239).[6,7] The (111) face was cleaved from the bulk structure to generate a slab containing 5 Cu-I layers. This surface was replicated in the *x* and *y* directions to generate a 4 x 4 x 1 supercell, and 30 Å of vacuum was inserted in the *z* direction. This resulted in lattice parameters of a=b=17.2534 Å and c=44.9678 Å, which were kept fixed in all geometry optimisations, while all atomic positions were allowed to relax.

The geometry of the clean surface was relaxed first, prior to adsorbing the helicene molecules. As noted previously, two surface terminations are possible, with the Cu-rich side undergoing a reconstruction[8]. The inequivalent sides of an optimised CuI slab. "Cu-rich" side and one unreconstructed side (see below figure).

Unreconstructed side
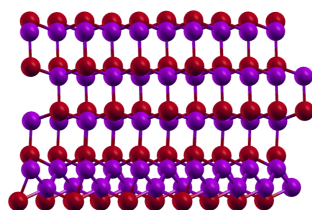

Cu-rich side

*a) The inequivalent sides of an optimised CuI slab. "Cu-rich" side and one unreconstructed side.*

The helicene molecules were then placed above the CuI surface in one of several orientations and the atomic positions once again relaxed. An additional geometry optimisation was performed for each of the isolated helicene molecules, in order to evaluate the adsorption energies.

Edge-on   **Flat lying**

C-H down   C-N down
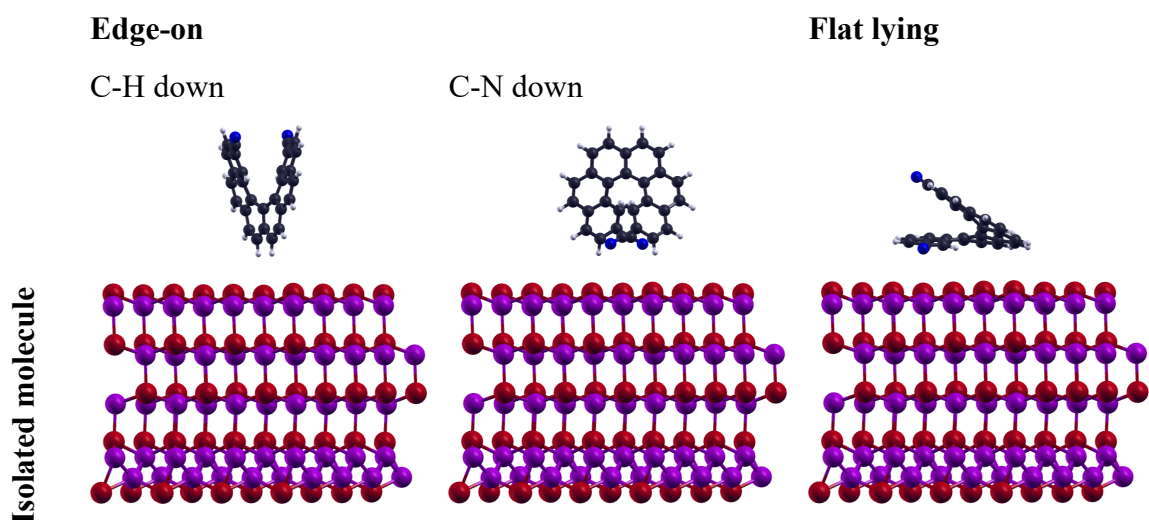
b) A cartoon depicting the helicene molecules placed above the CuI surface in edge and face-on configurations.

To determine whether the edge-on orientation of the CN6H on the CuI surface is unique to the CN6H (i.e., whether the CN group causes some preferential arrangement), the same calculations were performed for carbo-helicenes where X was C≡N, C≡CH and H.
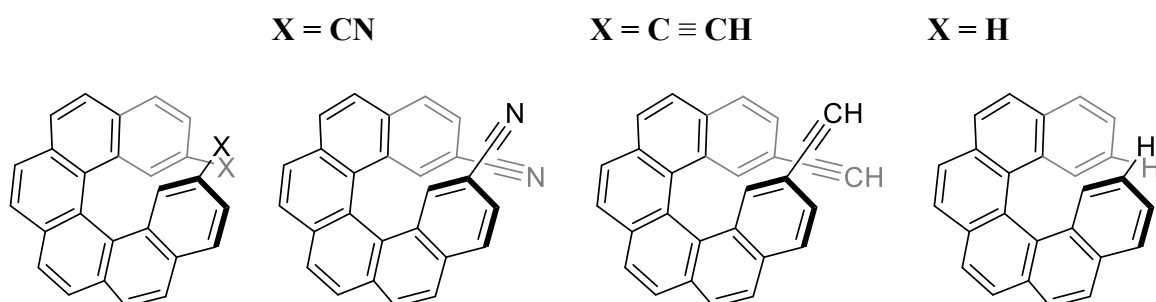
X = CN   **X = C ≡ CH**   **X = H**

c) Chemical structures of the helicene derivatives considered in these simulations.
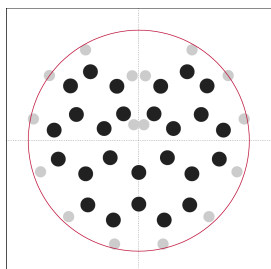
The adsorption energies (in eV) for the various geometries.

	Unreconstructed side			Cu-rich side		
	X = CN	X = C ≡ CH	X = H	X = CN	X = C ≡ CH	X = H
X up	− 0.48	− 0.41	− 0.34	− 0.33	− 0.41	− 0.32
X down	− 0.61	− 0.66	− 0.42	− 0.77	− 0.67	− 0.42
Flat-lying	− 1.17	− 1.16	− 0.87	− 1.13	− 1.17	− 0.86

Irrespective of the reconstructed CuI surface (Cu-rich or unreconstructed), the flat-lying orientation is always observed to be the most stable in these calculations, which we attribute to
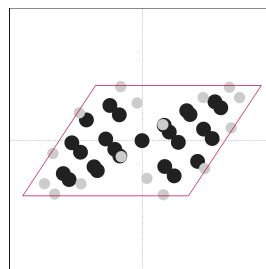
17

the large contact area and dispersion binding of this orientation. To account for the increased interfacial area of the flat-lying helicenes, we then normalised the binding area to the approximate area projected by the CN6H onto the CuI slab in the upright and flat-lying configurations of CN6H.

Flat-lying projection	**Edge-on projection**
Contact area ~ a circle of radius 5 Å à Area = **78.54 Å²**	Contact area ~ a parallelogram of 7.5 Å and height 5 Å à Area = **37.50 Å²**

c) Contact-area projections for flat-lying and edge-on molecular configurations.
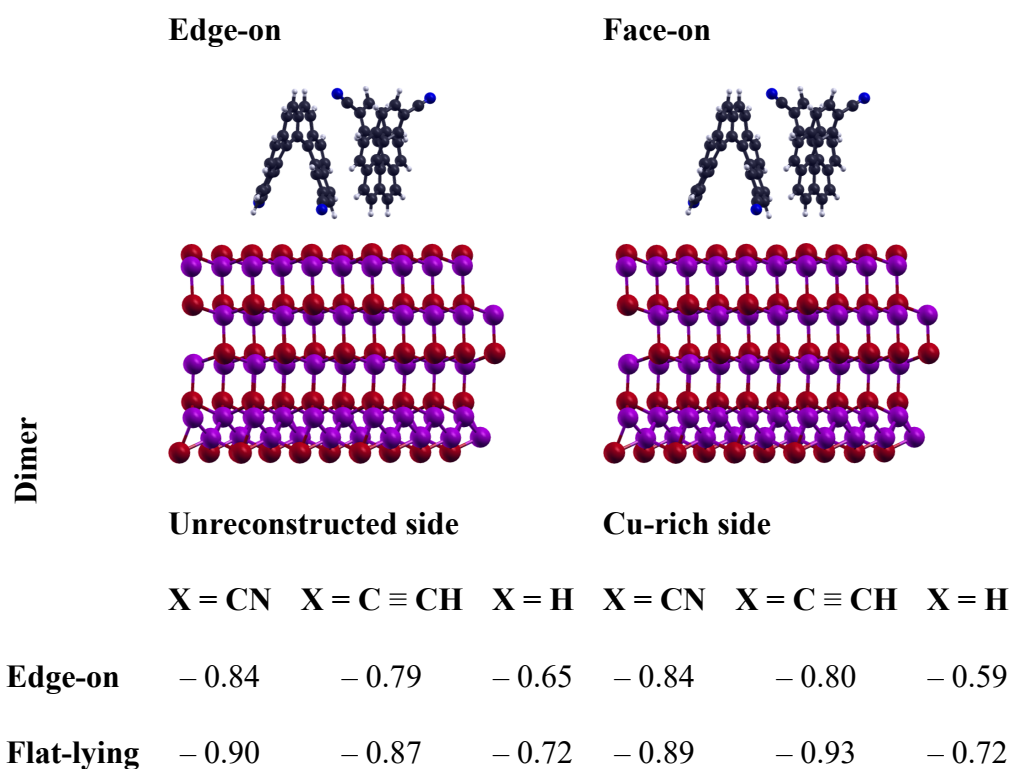
<u>Adsorption energies normalised by surface area (eV/ Å²) in the flat-lying and edge on configurations.</u>

	Unreconstructed side			**Cu-rich side**		
	X = CN	**X = C ≡ CH**	**X = H**	**X = CN**	**X = C≡CH**	**X = H**
X up	– 0.013	– 0.011	– 0.009	– 0.009	– 0.011	– 0.008
X down	– 0.016	– 0.018	– 0.011	– 0.020	– 0.018	– 0.011
Flat-lying	– 0.015	– 0.014	– 0.011	– 0.014	– 0.015	– 0.010

Therefore, once the surface area is accounted for, the edge-on orientation is lower in energy for the Cu-rich termination and also becomes much closer in energy for the unreconstructed termination (see optimised slab diagram). These results show that the orientation behaviour seen for CN6H on CuI is likely to occur in other functionalised carbo helicenes as the flat-lying/edge-on orientations become less/more energetically favourable.

As single molecule models cannot accurately predict the behaviour of supramolecular assemblies, we performed the same simulations for edge-on and flat-lying dimers. In this case, the edge-on CN6H orientation is considerably lower in energy than other functional groups for the unreconstructed surface. The results from these emphasises the complexity of

computational simulations as the intermolecular interactions stabilise the edge-on orientations relative to the flat-lying orientations for the case where X = CN, but destabilise in the case for X = C ≡ CH and X = H. It is likely that other helicenes will also have edge-on orientation on a CuI surface, but the nuanced balance of molecule-molecule and molecule-surface interactions makes it hard to predict with any certainty.

	Edge-on	Face-on
Dimer		

	Unreconstructed side			Cu-rich side		
	X = CN	X = C ≡ CH	X = H	X = CN	X = C ≡ CH	X = H
Edge-on	− 0.84	− 0.79	− 0.65	− 0.84	− 0.80	− 0.59
Flat-lying	− 0.90	− 0.87	− 0.72	− 0.89	− 0.93	− 0.72

To accompany these computational calculations, we investigated the molecular packing of racemic ET6H (X = C-CH) thin films on various templating layers experimentally. ET6H has two polymorphs, NEMKUO or PICFEO01. The NEMKUO structure belongs to a trigonal crystal system with hexagonal space group (P3$_2$21), and exhibits equivalent supramolecular columns to the UJOCOL crystal structure of CN6H. We grew 100 nm thin films of ET6H on the various templating layers (bare, PTCDA and CuI). Whilst we cannot use the chiroptical response to understand the molecular orientation (as the sample is racemic), the absorption, photoluminescence, Raman and XRD show clear differences depending on the choice of templating layer, indicating the molecular orientation of ET6H is controlled by the choice of templating layer, despite ET6H having no C≡N group. Understanding the molecular orientation is complicated by the polymorphism: the positions of the XRD peaks (e.g. on CuI 18.3°, 27.9°, 31.9°) indicate that the ET6H molecules adopt both polymorphs (NEMKUO and PICFEO01).

Despite this, the peak at 27.9°, which corresponds to the (3, -1, 0) plane and is common to both CN6H and ET6H, is indicative of edge-on packing.
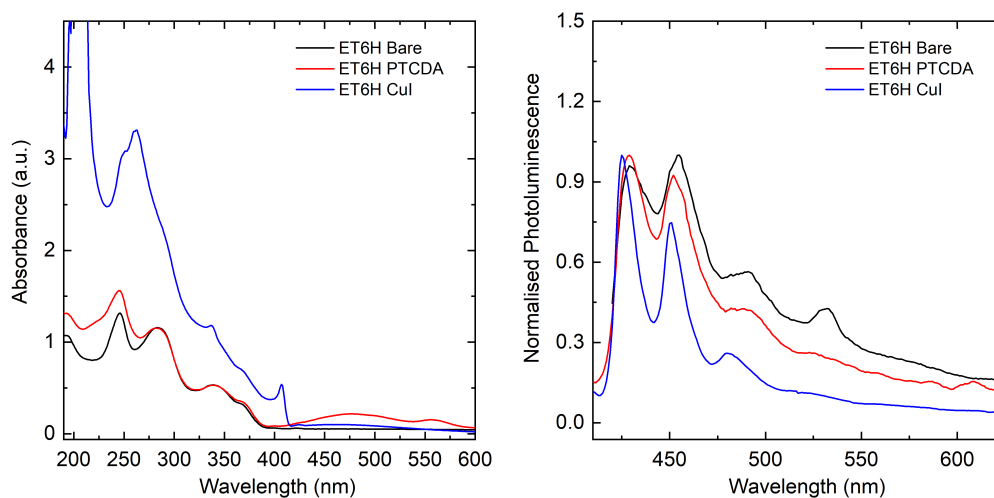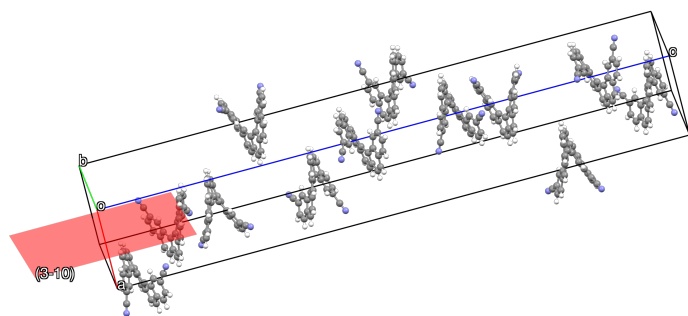

UV-Visible absorption and photoluminescence (λ_ex = 325 nm) spectra for 80 nm thick ET6H films on bare substrates (black), PTCDA-templated substrates (red) and CuI templated substrates (blue).
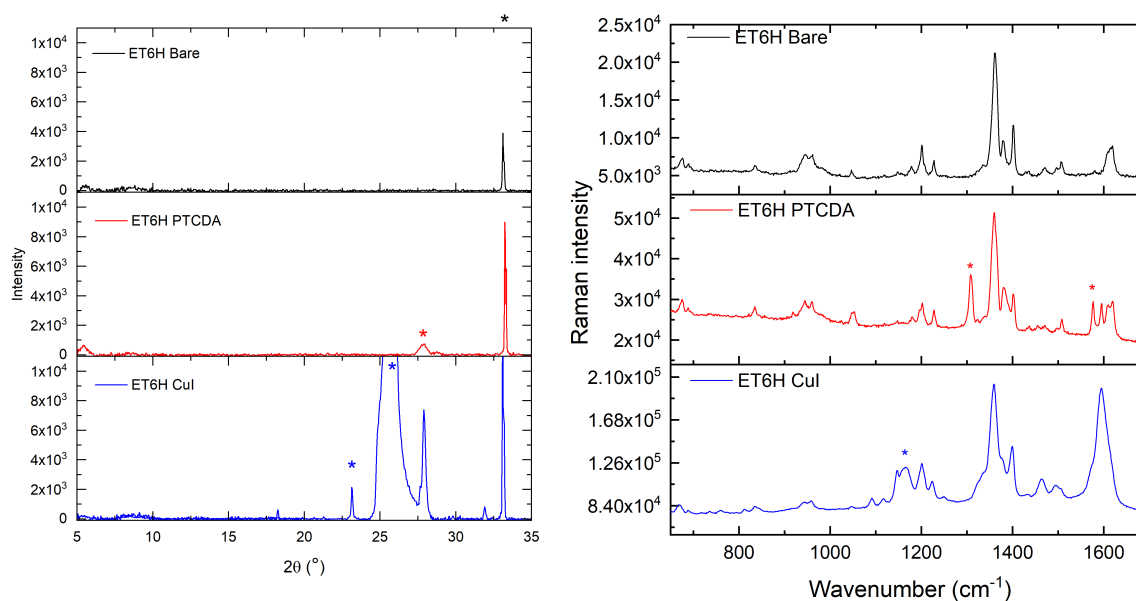
XRD patterns and Raman spectra (λ_ex = 633 nm) spectra for 80 nm thick ET6H films on bare substrates (black), PTCDA-templated substrates (red) and CuI templated substrates (blue).

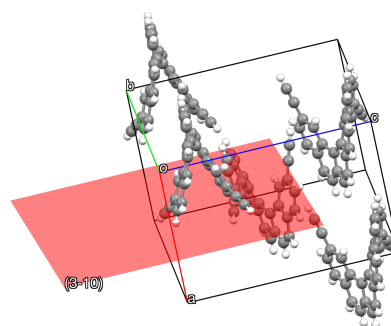*The (3, -1, 0) plane in the UJOCOL (CN6H) and NEMUKO (ET6H) crystal structure. Diffraction from this plane is present in the CuI templated thin films of CN6H and ET6H.*

We note that racemic thin films of CN6H adopt the same molecular packing as for the enantiopure, indicating that the approach should work for both racemic and enantiopure helicenes that can form supramolecular columns.
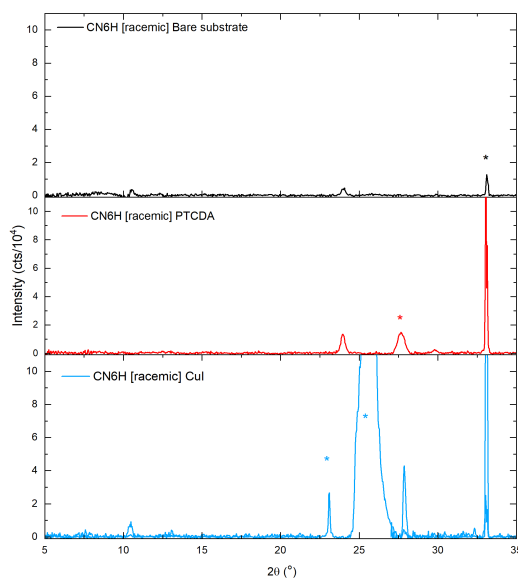
XRD patterns for 78 nm thick racemic CN6H films on bare substrates (black), PTCDA-templated substrates (red) and CuI templated substrates (blue).
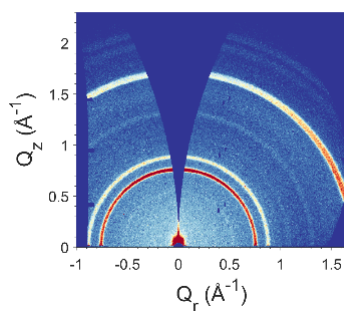
Supplementary Figure 5. Absorption and CD spectra and XRD of CN6H [*M*] thin films of various thicknesses.

To confirm the same molecular packing is achieved in thinner films (e.g., thicknesses comparable to those used as the charge injection layers of optoelectronic devices), we measured the UV-Visible absorption, circular dichroism and XRD of 10 and 42 nm CN6H [*M*] films. Note, that the 10 nm films were grown on quartz substrates, so do not display the high angle scattering peak (~ 33°) characteristic of silicon.
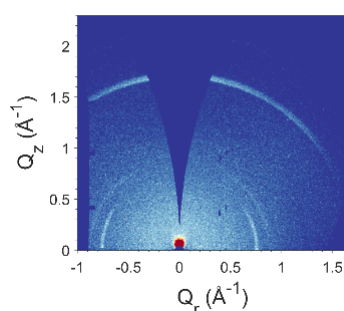
We also measured the GIWAXS patterns of 200 nm CN6H [*M*] films, which are comparable to the GIWAXS patterns of 78 nm CN6H [*M*] films reported in the manuscript.

*Experimental 2D GIWAXS diffraction patterns of untemplated and templated 200 nm thick films of **CN6H** [M].*
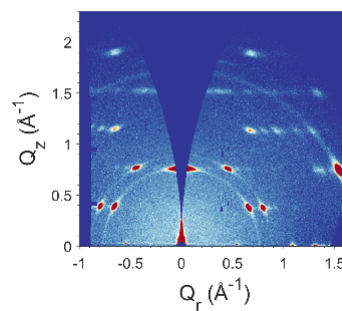
Bare Substrate   **PTCDA templated**   **CuI templated.**

Supplementary Figure 6. Absorption and CD spectra of CN6H [M] thin films pre- and post-annealing

To probe the temperature stability of the molecular orientation, we characterised the optical response of CN6H films before and after annealing the 78 nm CN6H [*M*] films at 95 °C for 3 hours. The UV-Vis and CD spectra are shown below and show negligible changes. This indicates that the supramolecular packing/molecular orientation is stable to temperature.
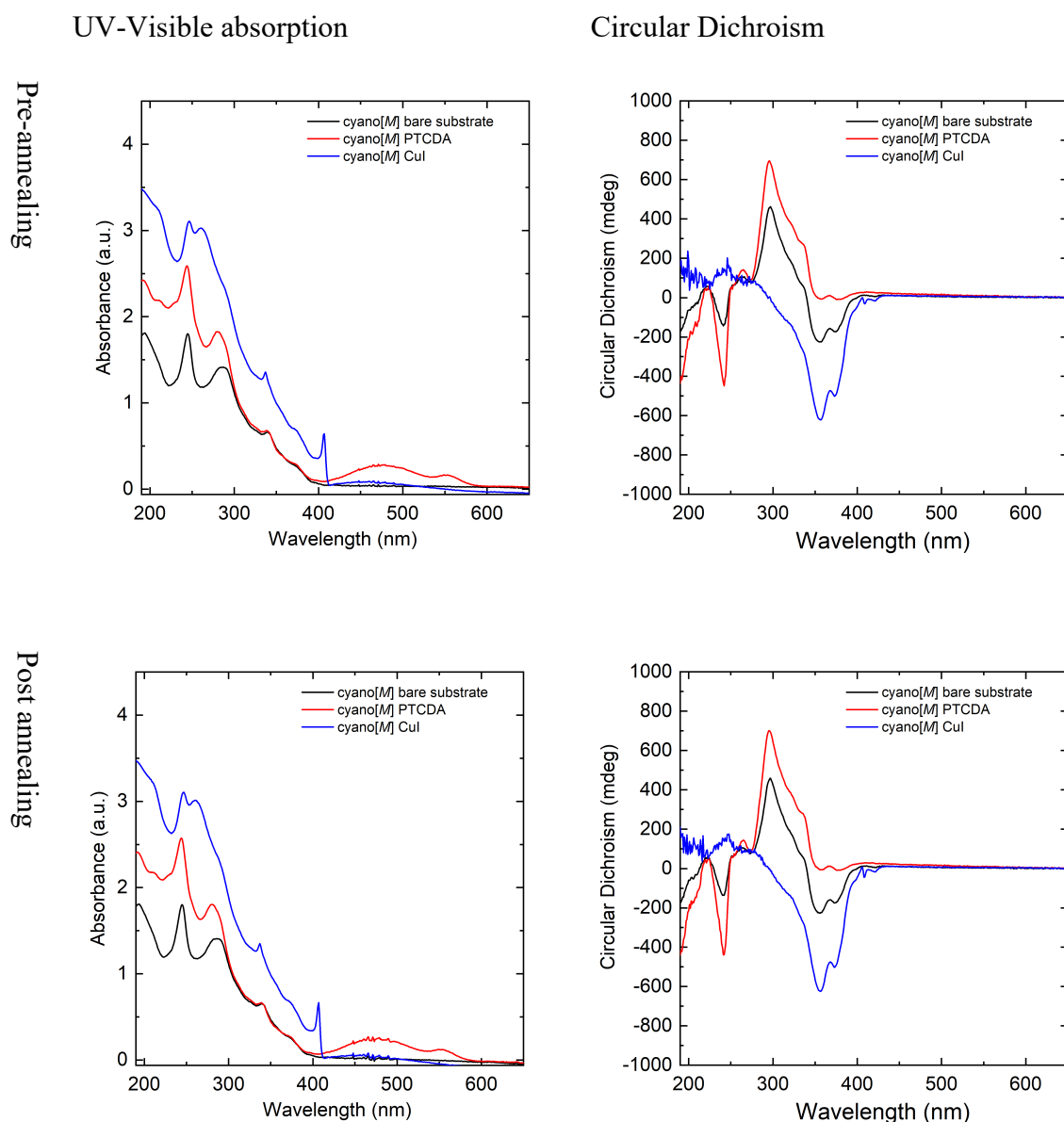
Supplementary Figure 7. CD spectra of untemplated and templated CN6H [*P*] thin films
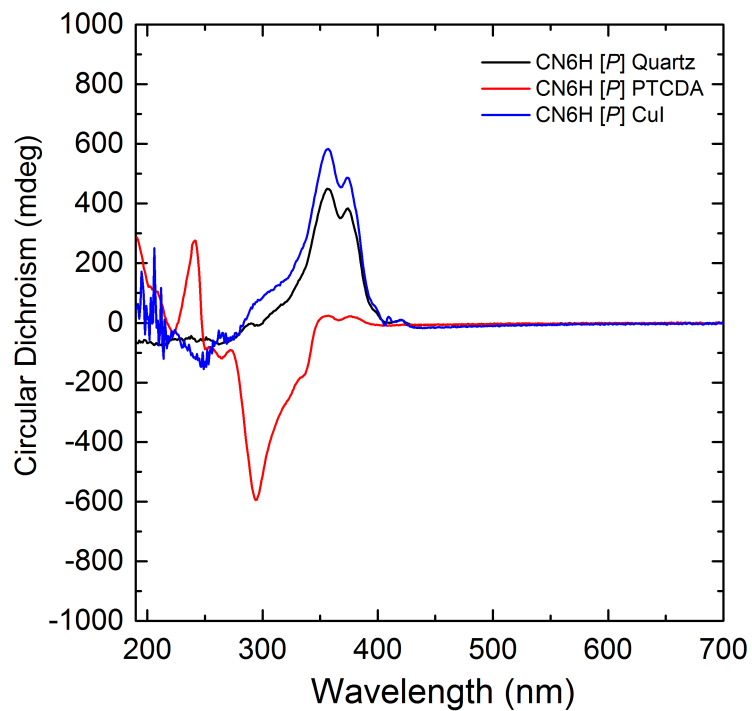
*Circular dichroism spectra of **CN6H** [*P*] thin films (thickness = 78 nm) on a non-interacting substrate (quartz, black line), 20 nm PTCDA (red) and 100 nm CuI (111) (blue line).*

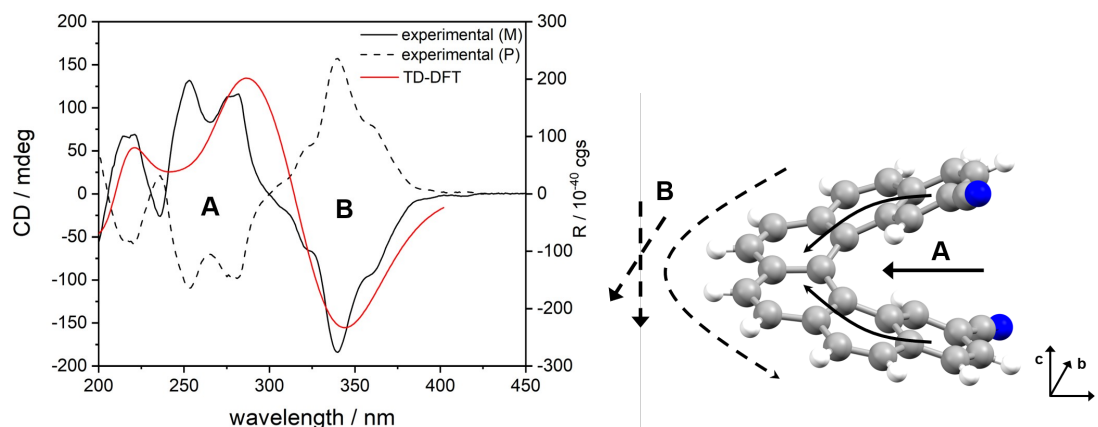**Supplementary Figure 8.** CD spectra of CN6H in solution

*Electronic Circular Dichroism spectra **CN6H** [M] in acetonitrile solution (2·10⁻⁵M) and simulated by TD-DFT at the B3LYP/6-31G level. Symmetry of the typical electronic transitions as described by Furche et al.[9] The continuous lines arrows indicate electron movement and total dipole components for A-symmetric transitions, oriented along the C2 axis of the helicene (a-axis). The dashed lines arrows indicate electron movement and total dipole components for B-symmetric transitions, oriented on the bc-plane, orthogonal to the C2 axis of the helicene.*

Supplementary Figure 9. CD spectra at various configurations

To monitor for evidence of linear artefacts, spectra were acquired in various configurations: with the thin film face-on to the detector, with the film rotated about the centre ('rotate') 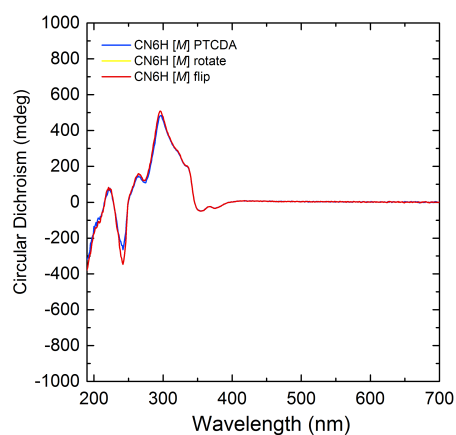and with the film facing away from the detector ('flip'). Circular dichroism spectra of **CN6H** [*M*] thin films (thickness = 78 nm) on:

Bare substrates:
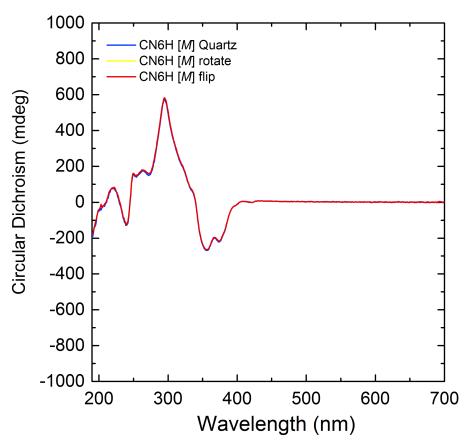
PTCDA:

CuI:
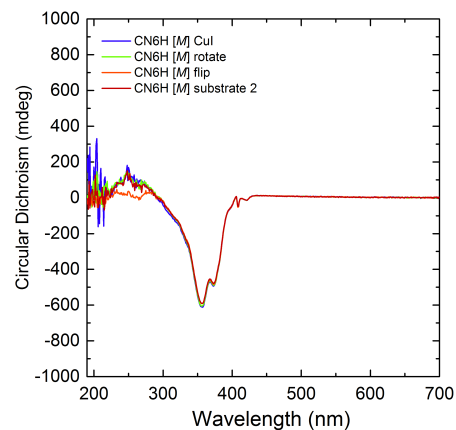
Supplementary Figure 10. Spatially resolved CD

Spatially resolved scans of CD intensity for templated and untemplated **CN6H** [*M*] thin films (thickness = 78 nm) acquired using the highly collimated synchrotron radiation of the Diamond Light Source.[10,11] The maps show the CD intensity (mdeg) as a function of position (step length, 50 μm) for the high (296 nm) and low (358 nm) energy bands. Note, only high (PTCDA) and low (CuI) energy bands were monitored for the templated **CN6H**.

High energy CD band (~ 296 nm)   **Low energy CD band (~ 358 nm)**
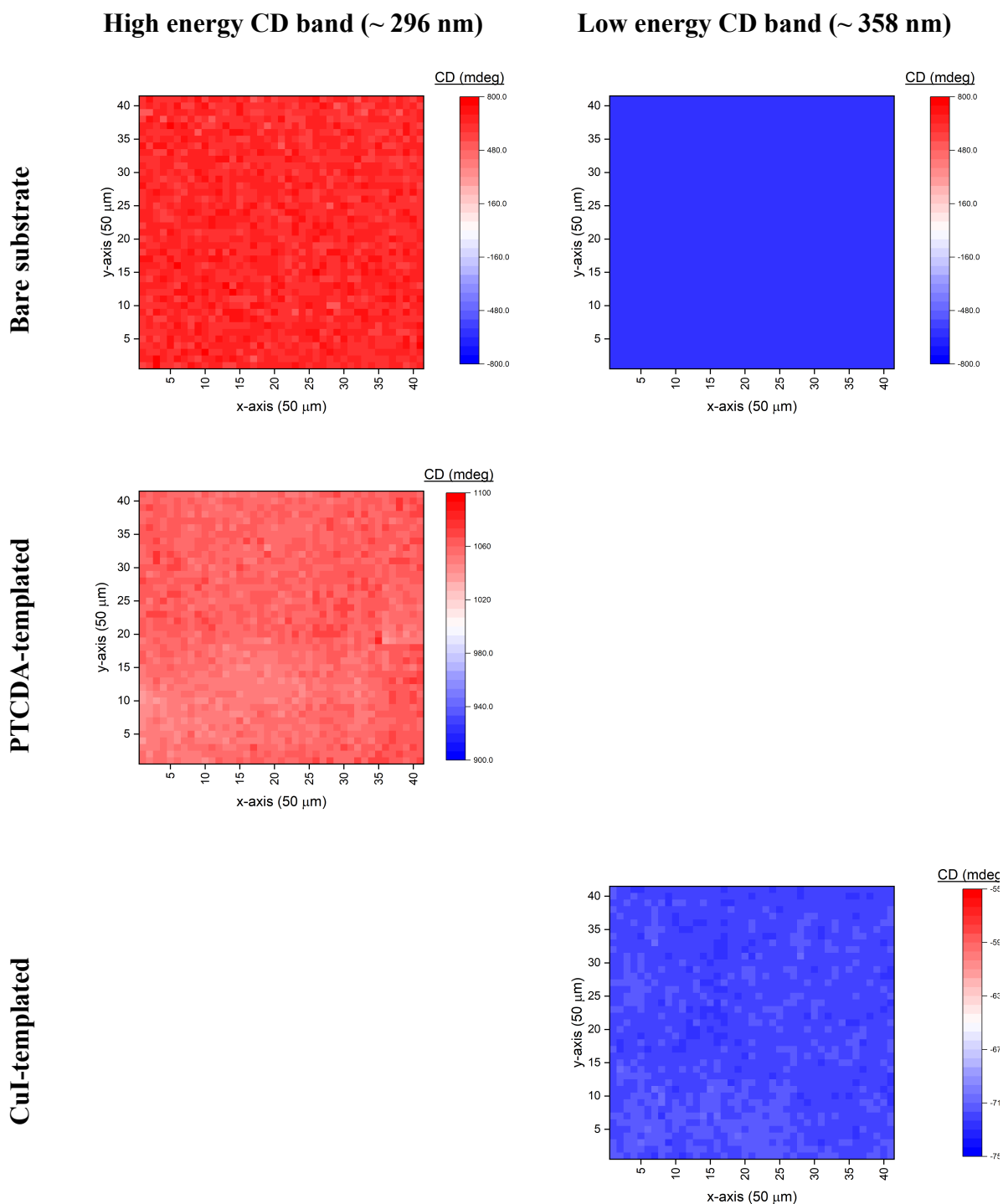
Supplementary Figure 11. Simulated CD and orientation-dependence

The first 20 optical transitions of the helicene were calculated in the gas phase using the resolution-of-identity coupled-cluster method RI-CC2 in Turbomole 7.5. The method delivers the 'right' and 'left' components of the electric dipole moment and angular momentum (magnetic dipole) moment in the cartesian directions indicated in Supplementary Figure 21.1. Ten of the states have A symmetry (moment directed along the z-axis of the molecule in that frame) and ten have B symmetry (moments lying in the x-y plane of the molecule).
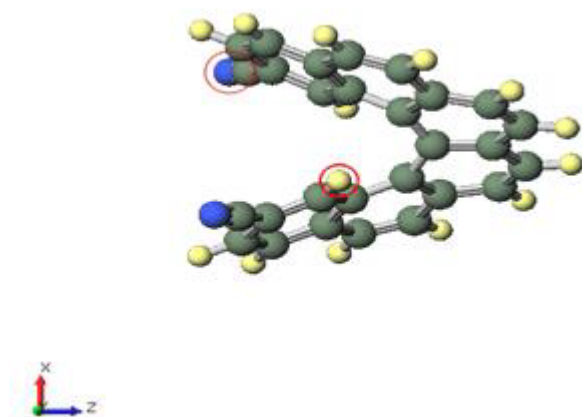

Figure S21.1: CN6H[M] molecule in the initial orientation (0, 0, 0) for TD-DFT simulations.

To obtain the rotatory strength and absorbance of the helicene placed in different orientations relative to the substrate we first rotate the frame of the molecule so that it adopts a lying (end rings of helicene cofacial with the substrate) or standing (π-system edge-on to the substrate) orientation and rotate all moments accordingly. To reproduce the PTCDA template situation, an average of the orientations (0°, 20°, 0°) and (0°, 0°, 20°) was used, while to reproduce the CuI template situation, an average of the orientations (0°, 90°, 0°) and (0°, 0°, 90°) was used. Here (α, β, γ) indicate the rotation angle around the x-, y- and z-axis.

We define the frame of the substrate such that the substrate lies in the y' z' plane and circularly polarised light incident in the x' direction. We then calculate the relevant components of the rotatory strength R and absorbance A for each transition, for this geometry. Thus for light incident along x' we require contributions from the y' and z' moments of the rotated molecule to the rotatory R and linear A transition strengths. We combine the life and right moments following:[12,13]

$$R = R_{y'} + R_{z'} \propto \mu_{ry'}m_{ly'} - \mu_{ly'}m_{ry'} + \mu_{rz'}m_{lz'} - \mu_{lz'}m_{rz'}$$

and

$$A = A_{y'} + A_{z'} \propto \left(\mu_{ry'}\mu_{ly'} + \mu_{rz'}\mu_{lz'}\right)E_t$$

Where E_t is the energy of the transition. We then sum the contributions from all 20 transitions in each case, broadening each spectral line into a Gaussian in energy space of width 0.25 eV. The resulting Circular Dichroism and Absorption spectra (represented by broadened oscillator strength lines) are shown in Supplementary Figure 21.2 (b) and (d) in comparison with the corresponding experimental spectra ((a) and (c)).
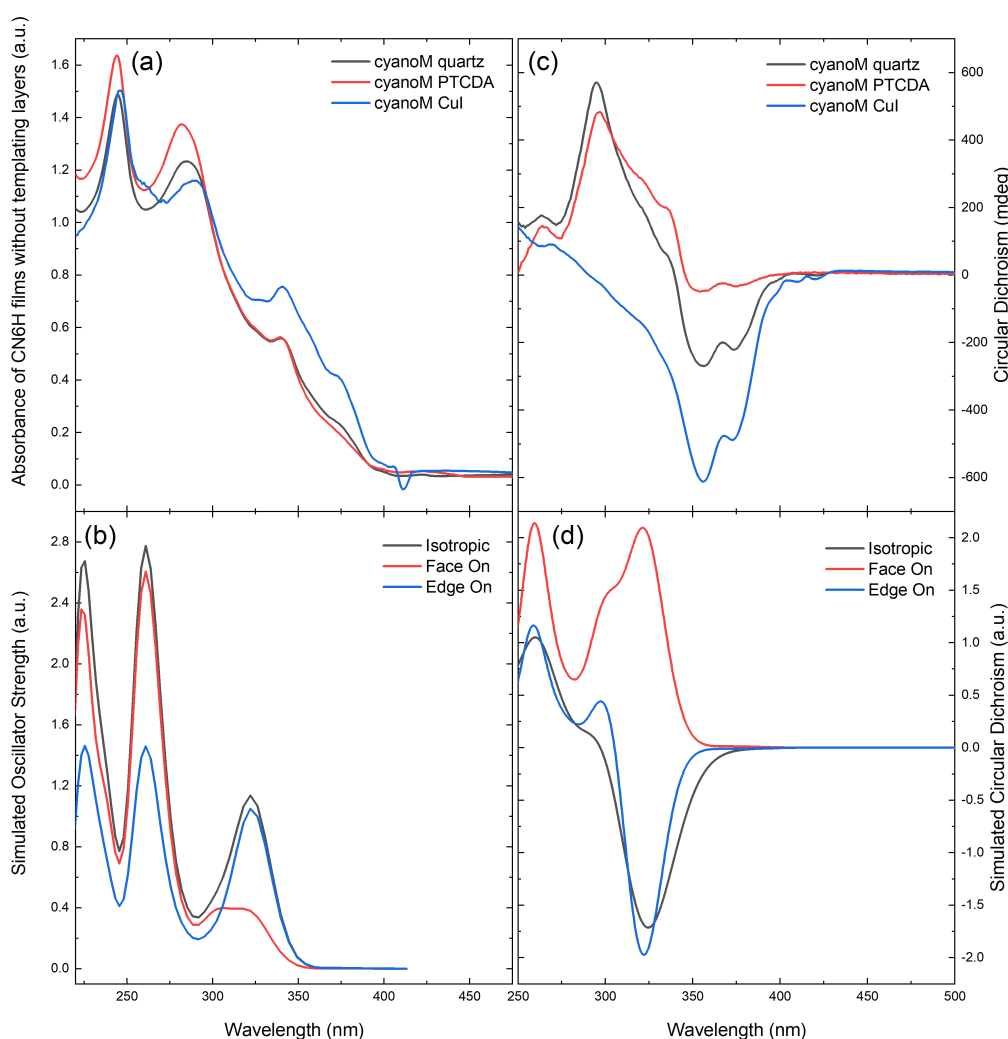

Figure 21.2: Experimental (a,c) and TD-DFT simulated (b,d) Absorption spectra (a, b) and Electronic Circular Dichroism (c, d) for the first 20 excited states of *CN6H [M]*. Random orientation, reproducing solution state or untemplated film, is represented by a dark grey line.

Edge on orientation, reproducing CuI template, is in blue. Face on orientation, reproducing PTCDA template, is in red.

All calculated transitions lie higher in energy than the experimental bands. Allowing for this shift, we observe a good agreement between calculated and experimental spectra. Both R and A spectra show a loss in intensity at shorter wavelength upon rotation from flat-lying to standing. This can be assigned to a loss in intensity of the A symmetry bands, which dominate the shorter wavelength part of the spectrum. At longer wavelength a single strong B transition (B3) dominates the spectra. Rotation from flat to standing reverses the sign of R in this region and enhances the strength of linear absorption. Both features are clearly evident in the experimental spectra. This supports our idea that the combination of CD and absorbance measurements together with orientation dependent calculations can serve as a probe of molecular orientation relative to a substrate or a probe beam.

Additionally, by comparing the simulated and experimental spectra we can see that the helicene on quartz appears to adopt an orientation more similar to the flat lying orientation than the isotropic orientation.

Transition energy /eV	Symmetry	Rx	Ry	Rz	Ax	Ay	Az
3.653	a1	0	0	-0.00141	0	0	0.000285
3.957	a2	0	0	0.032916	0	0	0.01113
4.107	a3	0	0	0.401752	0	0	0.108994
4.412	a4	0	0	0.048146	0	0	0.043186
4.636	a5	0	0	0.326694	0	0	0.254768
4.795	a6	0	0	0.66031	0	0	0.408597
5.075	a7	0	0	0.130217	0	0	0.0547
5.242	a8	0	0	0.467032	0	0	0.311015
5.455	a9	0	0	0.56345	0	0	0.123869
5.488	a10	0	0	0.558697	0	0	0.104082
3.307	b1	-0.01653	0.004965	0	0.00113	0.000168	0
3.836	b2	-2.83726	0.770194	0	0.303341	0.033991	0
4.218	b3	-0.1209	0.028164	0	0.006497	0.000751	0
4.418	b4	-0.11872	0.067529	0	0.018156	0.019433	0
4.482	b5	-0.00271	0.038164	0	0.006524	0.011945	0
4.627	b6	0.54821	-0.1107	0	0.005297	0.046952	0
4.775	b7	-0.133363	-0.08185	0	0.041675	0.244882	0
5.139	b8	-0.0595	-0.01613	0	0.012538	0.001881	0
5.401	b9	-0.38289	-0.06519	0	0.106586	0.002229	0
5.566	b10	0.018391	-0.83487	0	0.001276	0.575521	0

Table of the x,y,z components of the Rotatory strength (Rx, Ry, Rz) and the oscillator strength (Ax, Ay, Az) for the first 20 electronic transitions of a *CN6H[M]* oriented as in Figure SXX above.

References

1. de Vries, A. H. M., Mulders, J. M. C. A., Mommers, J. H. M., Henderickx, H. J. W. & de Vries, J. G. Homeopathic ligand-free palladium as a catalyst in the heck reaction. A comparison with a palladacycle. *Org. Lett.* **5**, 3285–3288 (2003).

2. Wachsmann, C., Weber, E., Czugler, M. & Seichter, W. New Functional Hexahelicenes − Synthesis, Chiroptical Properties, X-ray Crystal Structures, and Comparative Data Bank Analysis of Hexahelicenes. *European J. Org. Chem.* **2003**, 2863–2876 (2003).

3. Breiby, D. W., Bunk, O., Andreasen, J. W., Lemke, H. T. & Nielsen, M. M. Simulating X-ray diffraction of textured films. *J. Appl. Crystallogr.* **41**, 262–271 (2008).

4. Ogawa, T., Kuwamoto, K., Isoda, S., Kobayashi, T. & Karl, N. 3,4:9,10-Perylenetetracarboxylic dianhydride (PTCDA) by electron crystallography. *Acta Crystallogr. Sect. B Struct. Sci.* **55**, 123–130 (1999).

5. Heutz, S., Cloots, R. & Jones, T. S. Structural templating effects in molecular heterostructures grown by organic molecular-beam deposition. *Appl. Phys. Lett.* **77**, 3938–3940 (2000).

6. Gražulis, S. *et al.* Crystallography Open Database-an open-access collection of crystal structures. *J. Appl. Cryst* **42**, 726–729 (2009).

7. G Wyckoff, R. W., Posnjak, E. & Ralph G Wyckoff, B. W. *THE CRYSTAL STRUCTURES OF THE CUPROUS HALIDES.* https://pubs.acs.org/sharingguidelines.

8. Kecsenovity, E. *et al.* Solar Photoelectroreduction of Nitrate Ions on PbI 2 /CuI Nanocomposite Electrodes. (2020) doi:10.1002/solr.202000418.

9. Furche, F. *et al.* Circular dichroism of helicenes investigated by time-dependent density functional theory. *J. Am. Chem. Soc.* **122**, 1717–1724 (2000).

10. Albano, G. *et al.* Electronic circular dichroism imaging (CD i) maps local aggregation modes in thin films of chiral oligothiophenes. *New J. Chem.* **43**, 14584–14593 (2019).

11. Hussain, R., Jávorfi, T. & Siligardi, G. CD Imaging at High Spatial Resolution at Diamond B23 Beamline: Evolution and Applications. *Front. Chem.* **0**, 128 (2021).

12. Turbomole 2019 User's Manual, Section 10.4. (2019).

13. Hättig, C. & Köhn, A. Transition moments and excited-state first-order properties in the coupled-cluster model CC2 using the resolution-of-the-identity approximation. *J. Chem. Phys.* **117**, 6939–6951 (2002).

14. Jiang, Z. GIXSGUI: A MATLAB toolbox for grazing-incidence X-ray scattering data visualization and reduction, and indexing of buried three-dimensional periodic nanostructured films. *J. Appl. Crystallogr.* **48**, 917–926 (2015).